

# Structural, Electrical, and Optical Properties of R-Type Hexagonal Ferrites Investigating the Effects of V+2 Substitutions

Zeeshan Ahmad<sup>1</sup>, Muhammad Tanveer<sup>2</sup>, Muhammed Arslan<sup>1</sup>, Maryam Shafat<sup>1</sup>,  
Muhammad Awais Shahid<sup>3</sup>

## ABSTRACT

The divalent transition element V<sup>+2</sup> substituted Sr<sub>1-x</sub>V<sub>x</sub>Mn<sub>2</sub>Fe<sub>4</sub>O<sub>11</sub> (x= 0.0, 0.1, 0.2, 0.3, 1.0) R-type hexagonal ferrite has been synthesized by employing sol gel auto-combustion method. The effect of substitution of V<sup>+2</sup> on the structural, electrical, and optical properties was studied by using X-ray diffractometer, and Fourier transform infrared spectrometer (FTIR) and Multiferroic test system. X-ray diffraction (XRD) analysis verified the presence of a pure R-type hexagonal ferrite phase. The substitution of V<sup>+2</sup> led to variations in the lattice parameters (a and c), with crystallite sizes ranging from 9.14 to 9.71 nm across all samples. The FTIR spectra revealed trace amounts of moisture and nitrogen, likely absorbed from the surrounding atmosphere. The P-E loops indicated the loopy behavior. The saturation and remanence polarization also altered with V<sup>+2</sup> substitutions.

**Keywords:** R-type hexa ferrites, Polarization, FT-IR spectroscopy, Electrical Properties.

magnetolectric properties, which are closely linked to the nanostructure and nanoparticles of the materials [2]. Hexagonal ferrites can be categorized into various classes, including M, X, Y, W, U, R, Z, and  $\beta$  types, based on their chemical formulas and crystal structures [3, 4]. Recently, within the hexagonal ferrite family, R-type hexagonal ferrites have garnered increasing attention due to their applications in switching, sensing for high-frequency uses, and in high-frequency dielectric resonators [5, 6]. The primary distinction between various types of hexagonal ferrites lies in the arrangement of their fundamental building blocks (S, R, and T) within their crystal lattices [7]. In the crystal lattice of R-type hexagonal ferrites, the sole basic block, denoted as 'R,' is present and arranged in a stacking pattern of RR\*, with R\* indicating a 180° rotation of the block along the c-axis, as depicted in Figure 1. The characteristics of R-type hexagonal ferrites can be altered by introducing substitutions of both

## 1. Introduction

In contemporary times, hexagonal ferrites have gained extensive utilization in the realm of magnetic materials and nano-electromagnetic devices [1]. In essence, ferrites represent ceramic materials. They are magnetic materials primarily comprised of oxides in which ferric ions play a dominant role. These materials are characterized by their insulating nature, exhibiting high electrical resistivity, low eddy current losses, and notable dielectric properties. Additionally, ferrites exhibit characteristics such as high saturation magnetization, high permeability, and moderate permittivity. In recent times, ferrite multiferroic materials have garnered increased attention due to their unexpected and intriguing structural and

divalent and trivalent elements into the interstitial sites of their crystal lattices [8]. Hence, the choice of the synthesis technique becomes pivotal in modifying the diverse properties of hexagonal ferrites. The sol-gel auto-combustion method stands out as particularly suitable, given its cost-effectiveness, which demands relatively inexpensive precursor salts for material synthesis [9]. Additionally, the size of the particles, the degree of crystallinity, composition, and the occupation of specific sites within the structure all play crucial roles in influencing the structural, electrical, and optical properties of R-type hexagonal ferrites. [7]. Consequently, the choice of the synthesis method becomes pivotal for modifying the diverse properties of hexagonal ferrites. In the current research, the sol-gel auto-combustion method was employed for synthesizing all the samples. It is worth noting that R-type hexagonal ferrites with V+2 substitution (coordination number = 6) have been rarely reported in the existing body of knowledge reported earlier up to our knowledge. This choice of material was the primary motivation for the current study. The research was designed to substitute the divalent base element, 'Sr<sup>2+</sup>,' with another divalent element, 'V<sup>2+</sup>,' across varying compositions (X = 0.0, 0.1, 0.2, 0.3, 1.0). The main objective was to explore and comprehend the significant impact of V<sup>2+</sup> on the structural, electrical, and FTIR properties of Sr<sup>2+</sup>-based R-type hexagonal ferrites.

## 2. Experimental procedure

R-type hexagonal ferrites with the general chemical formula Sr<sub>1-x</sub>V<sub>x</sub>Fe<sub>4</sub>Sn<sub>2</sub>O<sub>11</sub>, where x takes values of 0.0, 0.1, 0.2, 0.3, and 1.0, were synthesized using the sol-gel auto-combustion method. Initially, an aqueous solution of the substituents was prepared by mixing various stoichiometric ratios of Sr(NO<sub>3</sub>)<sub>2</sub>, Sn(NO<sub>3</sub>)<sub>2</sub>·6H<sub>2</sub>O, V(NO<sub>3</sub>)<sub>2</sub>·6H<sub>2</sub>O, iron nitrate, and citric acid in deionized water. Separate beakers were used for preparing these solutions with varying concentrations of the substituents. The solutions were placed on hot plates within an ESCO fume hood for stirring and heating. Potassium hydroxide (KOH) was added dropwise to each solution to maintain a pH level in the range of 7 to 8 during stirring. After heating at 80 °C with continuous stirring for 4 hours, a viscous brown-colored gel was formed. The gel was then heated for 15 minutes to produce ash, which was subsequently sintered at 800 °C in a box furnace for 3 hours. The resulting product was ground into a fine powder using an agar mortar and pestle for 20 minutes. The ground powder was then compressed into small pellets using a hydraulic press with a force of 40 kN. These pellets were employed for characterization, including the assessment of electrical polarization properties, X-ray diffraction (XRD), and FTIR properties. Structural properties were determined using a Bruker D8 advance X-ray diffractometer with a CuK $\alpha$  source and a wavelength of  $\lambda = 1.54 \text{ \AA}$ . The dielectric properties, varying with frequency in the range of 20 Hz to 20 MHz, were evaluated using a Wanyer impedance analyzer, model # 6500 B series, at room temperature. FTIR spectra were acquired utilizing a Shimadzu IR Tracer 100, spanning the wavenumber range from 4000 to 400 cm<sup>-1</sup>. For the measurement of electrical polarization properties in the

Multiferroic II Ferroelectric) was employed.

## Results and Discussion

### 3. Structural Properties (XRD)

The XRD patterns of  $Sr_{1-x}V_xMn_2Fe_4O_{11}$  ( $x=0.0, 0.1, 0.2, 0.3, 1.0$ ) of R-type hexagonal ferrites, sintered at  $800^\circ\text{C}$  are represented in figure below.

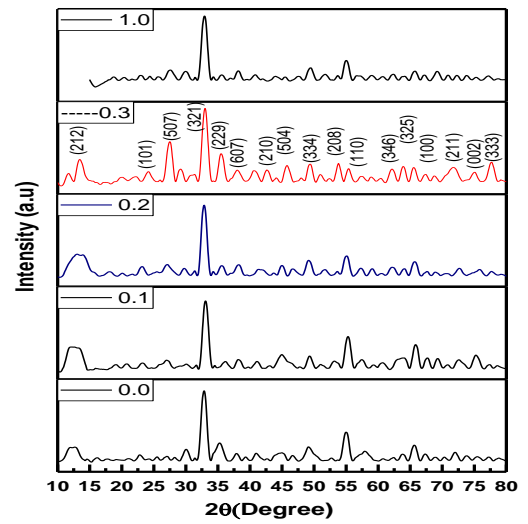


Figure.1(b). XRD pattern of  $Sr_{1-x}V_xMn_2Fe_4O_{11}$  R-type hexagonal ferrite  $X=(0.0, 0.1, 0.2, 0.3, 1.0)$

**Table 1** Structural parameter of (  $Sr_{1-x}V_xMn_2Fe_4O_{11}$  ) R-type hexagonal ferrites.

Concentration	a(A°)	c(A°)	c/a	V <sub>cell</sub> (A°) <sup>3</sup>	CrystalliteSize(nm)	Bond length(A°)
X=0.0	5.25	9.29	1.43	223	9.54	4.75
X=0.1	5.58	12.43	1.77	528	9.65	6.35
X=0.2	5.55	11.13	2.00	298	9.71	5.64
X=0.3	5.56	10.83	1.94	291	9.62	5.50
X=1.0	5.69	12.04	2.11	338	9.14	6.08

$$V=0.866a^2c \quad (2)$$

The formation of single-phase hexagonal ferrites in all the synthesized samples was verified by comparing them with the JCPDS reference card #771506, which exhibits a space group of p6/mmc. No impurity groups were detected. However, in the case of the x=0.3 concentration, additional peaks at 2θ values of 53.8°, 71.8°, and 77.6° emerged, which can be attributed to R-type hexagonal ferrites and were confirmed through the JCPDS pattern. Furthermore, a peak at 2θ value 30.49° for x=0 exhibited a 0.5° shift from the JCPDS pattern and disappeared in the substituted sample. Such peak shifts are a common occurrence in R-type hexagonal ferrites. It is evident that all the observed peaks in the XRD patterns correspond to the hexagonal structure, with no additional peaks indicating the presence of residual or extraneous materials [3]. Figure 4.1 reveals that the peak intensities are influenced by the substitution of V<sup>2+</sup>. Moreover, the graph illustrates that certain peaks emerge while others diminish with the introduction of V<sup>2+</sup> substitutions. It is noteworthy that all these observed peaks are consistent with the R-type hexagonal structure [7].

The lattice parameters (a & c) and their ratio (a/c) were determined using the following formula;

$$\sin^2\theta = \frac{\lambda^2}{3a^2}(h^2+hk+k^2) + \frac{\lambda^2}{4c^2}(l^2) \quad (1)$$

The unit cell volume and crystallite size were calculated from the XRD data and are tabulated in Table 4.1. The unit cell volume was computed using the formula:

the lattice parameters were observed to increase with substitution of V<sup>2+</sup> contents. The variation observed in lattice parameters may be due to the difference in ionic radius of Fe<sup>+3</sup>(0.64Å) and v<sup>2+</sup> (2.05Å). The bond length was calculated by the formula;

$$BL = \sqrt{\left(\frac{a}{3}\right)^2 + (0.5 - u)^2 c^2} \quad (3)$$

where u is positional parameter and calculated with the help of this equation

$$u = \frac{a^2}{3c^2 + 0.25} \quad (4)$$

the crystallite size was calculated from the Scherer formula;

$$D = \frac{0.94\lambda}{FWHM \cos\theta} \quad (5)$$

0.94 is shape constant, λ is the wavelength of x-ray source, FWHM shows the peak width at half maxima and θ is the angle, the calculated bond lengths showed variation with the substitution of V<sup>2+</sup> sample with x=1.0 has bond length 6.08Å, the sample with concentration x=0.3, x=0.2, x=0.1, x=0.0 have the bond length 5.50Å, 5.64Å, 6.35Å, 4.75 Å respectively. The increase in crystallite size for all samples ranged from 9.14 Å to 9.71 Å to be observed from the table 4.1. the small variation is observed due to the bond energy of V<sup>2+</sup> O<sup>2-</sup> lower than the Fe<sup>3+</sup>O<sup>2-</sup> bond energy[10]. The dislocation density was calculated by the following relation.

$$D=1/S^2 \quad (6)$$

when the ion of  $V^{2+}$  substitute the  $Fe^{3+}$  in hexagonal ferrites it consumes less energy than  $Fe^{3+}$  and results in the decrease of crystallite size[11].

#### 4. Electrical polarization

In Figure 4.2, the Electric Field vs. Polarization graphs for all values are presented. Notably, polarization increases in the positive electric field region while decreasing in the negative electric field regions. This behavior can be attributed to factors such as leakage current or instability in the negative pole [3]. The values for both types of polarization, namely saturation ( $P_s$ ) and remanence ( $P_r$ ), have been provided in Table 4.2. Notably, at  $x=1.0$ , the saturation polarization ( $P_s$ ) exhibits a notably higher value at 9.99, in contrast to the other samples ( $x=0.0, 0.1, 0.2, 0.3$ ). This behavior can be attributed to an increase in leakage current, which reduces the material's resistivity and consequently lowers  $P_r$  and  $P_s$  values. This phenomenon may be associated with the increased randomness of

crystallite structure[12, 13]. The loosy behavior increased at ( $x=1.0$ )

and then decreased. It was noted that the highest value of P-E loops at ( $x=1.0$ ) show the loss in resist at ( $x=1.0$ ). Table 4.2 also indicates that the saturation polarization ( $P_s$ ) for all values consistently exhibits higher values compared to remanence polarization ( $P_r$ ). This characteristic aligns with the expected condition for hysteresis loops in materials with losses [14]. Table 4.2 reveals a consistent trend where the saturation polarization ( $P_s$ ) for all the samples surpasses the remanence polarization ( $P_r$ ). This aligns with the anticipated condition for materials exhibiting hysteresis loops with losses. Notably, one of the distinctive attributes of the material synthesized in this study is its ferroelectric properties, which hold significant importance for the electronics industry. It is anticipated that this synthesized material is well-suited for magneto-dielectric coupling applications [15].

**Table 4.2** Saturation ( $P_s$ ) and remanence polarization ( $P_r$ ) values for all  $V^{+2}$  substituted samples at room temperature.

Serial No.	Concentration X	Saturation polarization $P_s$	Remanence polarization $P_r$	Resistivity $\rho$ ( $\Omega$ -cm)
1	0.0	6.52	3.99	$3.7 \times 10^7$
2	0.1	4.43	4.26	$7.4 \times 10^7$
3	0.2	1.18	1.05	$0.6 \times 10^7$
4	0.3	7.93	5.28	$0.9 \times 10^7$
5	1.0	9.99	7.39	$0.3 \times 10^7$

### 4.3 Fourier transform infrared spectroscopy (FTIR) analysis

To analyze the phases present in the material, FTIR analysis was conducted on all V+2 substituted R-type hexagonal ferrites, as depicted in the figure 3 below. The FTIR spectra reveal multiple bands. Notably, the absorption band at  $3731\text{ cm}^{-1}$  corresponds to the H-O-H bond, indicating the presence of moisture within the material [16]. The prominent feature observed at  $1132\text{ cm}^{-1}$  can be attributed to the presence of carbon (C) and oxygen (O) atoms and their combination in the sample, suggesting a stretching vibration of the C-O bond. This observation suggests that the carbon was absorbed from the atmosphere[17]. The peak observed at  $993\text{ cm}^{-1}$  is a result of the stretching vibration of the carbon-hydrogen (C-H) bond [18]. The peak observed at  $669\text{ cm}^{-1}$  can be attributed to the presence of nitrogen, which was introduced into the material from the surrounding air [19]. The peak at  $422\text{ cm}^{-1}$  can be attributed to the stretching vibration of metal-oxygen (Fe--O--Fe) bonds, which is a typical characteristic of hexagonal ferrites [20]. The absence of any additional bands in the FTIR spectra can be attributed to the absence of impurities. This confirms that the material under study consists of a single hexagonal phase [21].

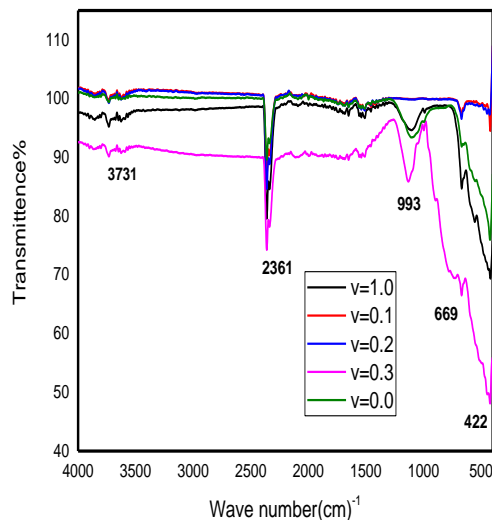


Figure.3. FTIR spectra of  $(\text{Sr}_{1-x}\text{V}_x\text{Mn}_2\text{Fe}_4\text{O}_{11})$  at  $(X=0.0, 0.1, 0.2, 0.3, 1.0)$  R-type hexagonal ferrites.

### 4.4 Electrical resistivity

The electrical properties of both pure and V+2 substituted samples were assessed within a voltage range of 0 to 200 V at room temperature. The resistivity was determined using the formula

$$R = \rho L / A$$

Here, 'A' represents the surface area of the sample, 'R' denotes resistance calculated from the plotted graphs, and 'L' indicates the thickness of the pellet. The changes in electrical resistivity concerning V2+ concentration within the range of 0 to 200V were graphically represented for all the samples. The specific resistivity values for these samples are detailed in Table 2. Observations indicate that

the resistivity of the samples initially increased and then decreased with the introduction of  $V^{2+}$  substitutions. Notably, the sample with a concentration of  $x = 0.1$  exhibited the lowest resistivity among all the samples. This decrease in resistivity can be attributed to increased conductivity, potentially resulting from electron hopping between  $Fe^{2+}$  and  $Fe^{3+}$  ions at octahedral sites. [22]. Based on the prior electrical polarization results, it was anticipated that the sample with  $x = 0.1$  would exhibit the highest conductivity among all the synthesized samples. Thus, the polarization and resistivity results are in excellent agreement with each other. Furthermore, materials with higher resistivity are of significance for applications in microwave absorption devices and transformers, as they help reduce eddy current losses [23].

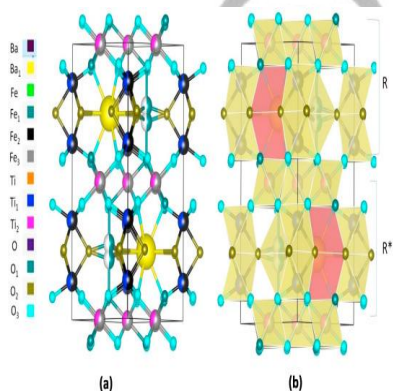


Figure 1 (a) The unit cell of R-type hexagonal ferrites indicating the occupation of different ions at different sites and bonding between these ions. (b)The stacking of R

## Conclusion

The divalent transition element " $V^{+2}$ " substituted  $Sr_{1-x}V_xMn_2Fe_4O_{11}$  ( $x= 0.0, 0.1, 0.2, 0.3$  and  $1.0$ ) R-type hexagonal ferrites was prepared by sol-gel auto combustion method. The single phase was confirmed for all samples through the XRD analysis. The lattice parameters ( $a$  and  $c$ ) were increased with  $V^{+2}$  content. The absence of any extra band due to any other or residual material in FTIR spectra also confirmed the single phase for all samples. The P-E loops of all samples indicated the loopy behavior. The electrical polarization has been increased in the area of positive electric field and decreased in the negative field region for all samples.

### Author statement

This work was designed on the basis of substitution of divalent element Sr with another divalent transition element " $V$ " and to understand the effect of this substitution on different properties of R-type hexagonal ferrites.

### Declaration of competing interest

The authors declare that they have no known competing financial interests or personal relationships that could have appeared to influence the work reported in this paper.

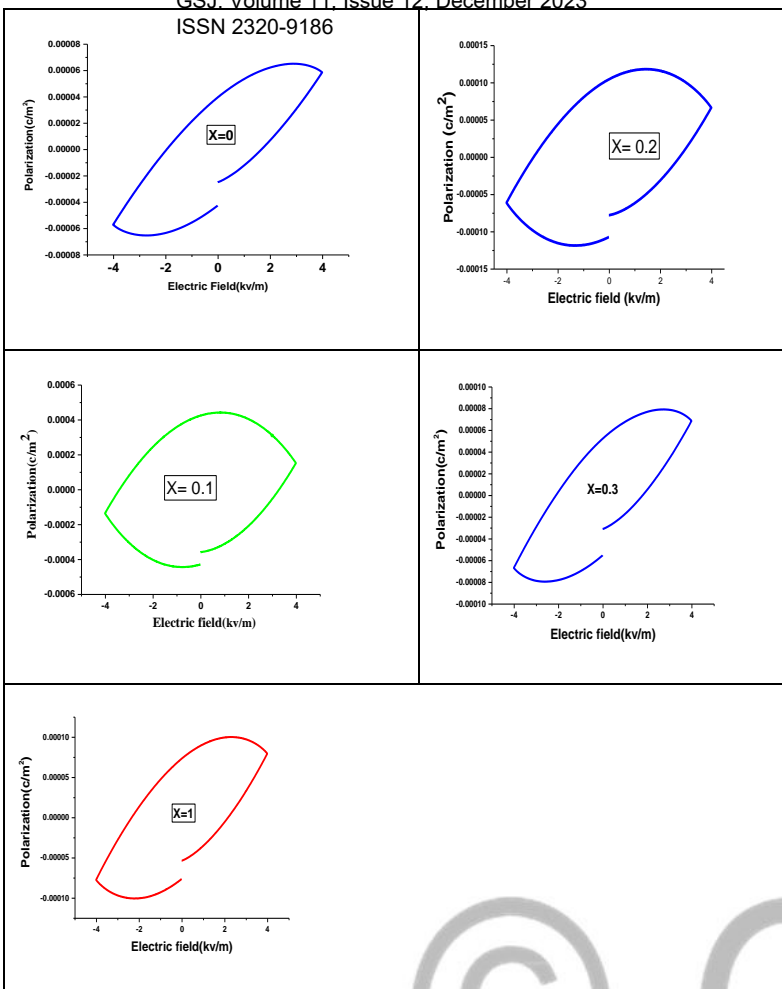


Figure.4.2. The P-E loop for  $(\text{Sr}_{1-x}\text{V}_x\text{Mn}_2\text{Fe}_4\text{O}_{11})$  R-type hexagonal ferrite at  $X = (0.0, 0.1, 0.2, 0.3, 1.0)$

## References

- [1] P. N. Dhruv *et al.*, "Investigation of structural, magnetic and dielectric properties of gallium substituted Z-type  $\text{Sr}_3\text{Co}_2\text{-xGa}_x\text{Fe}_24\text{O}_41$  hexaferrites for microwave absorbers," *Journal of Alloys and Compounds*, vol. 822, p. 153470, 2020.
- [2] N. A. Spaldin and R. Ramesh, "Advances in magnetoelectric multiferroics," *Nature materials*, vol. 18, no. 3, pp. 203-212, 2019.
- [3] M. Amini and A. Gholizadeh, "Shape control and associated magnetic and dielectric properties of  $\text{MFe}_{12}\text{O}_{19}$  (M= Ba, Pb, Sr) hexaferrites," *Journal of Physics and Chemistry of Solids*, vol. 147, p. 109660, 2020.
- [4] X. Zhang and J. Zhang, "Synthesis and magnetic properties of  $\text{Ba}_2\text{Fe}_{14}\text{O}_{22}$  Y-type hexaferrite," *Materials Letters*, vol. 269, p. 127642, 2020.
- [5] T. Amjad, I. Sadiq, A. B. Javaid, S. Riaz, S. Naseem, and M. Nadeem, "Investigation of structural, electrical, electrical polarization and dielectric properties of CTAB assisted  $\text{Ni}^{2+}$  substituted R-type nano-hexaferrites," *Journal of Alloys and Compounds*, vol. 770, pp. 1112-1118, 2019.
- [6] M. Shahbaz *et al.*, "Peculiar magnetic behavior and structural, electrical, dielectric properties of substituted R-type hexagonal ferrites," *Journal of Magnetism and Magnetic Materials*, vol. 499, p. 166309, 2020.
- [7] N. Yasmin *et al.*, "Impact of Ho-Ni substitution on structural, morphological and dielectrical characteristics of  $\text{BaFe}_{12}\text{O}_{19}$  M-type hexagonal ferrite," *Physica B: Condensed Matter*, vol. 581, p. 411950, 2020.
- [8] R. C. Pullar, "Hexagonal ferrites: A review of the synthesis, properties and applications of hexaferrite ceramics," *Progress in Materials Science*, vol. 57, no. 7, pp. 1191-1334, 2012.
- [9] T. W. Mammo *et al.*, "Synthesis, structural, dielectric and magnetic properties of cobalt ferrite nanomaterial prepared by sol-gel

- autocombustion technique," *Physica B: Condensed Matter*, vol. 581, p. 411769, 2020.
- [10] A. ur Rehman, S. Shaikat, M. N. Akhtar, and M. Ahmad, "Evaluations of structural, magnetic and various dielectric parameters of Ni-substituted Zn<sub>2</sub>W-type hexagonal ferrites for high frequency (1–6 GHz) applications," *Ceramics International*, vol. 45, no. 18, pp. 24202-24211, 2019.
- [11] A. R. Kagdi *et al.*, "Influence of Mg substitution on structural, magnetic and dielectric properties of X-type bariumzinc hexaferrites Ba<sub>2</sub>Zn<sub>2-x</sub>MgxFe<sub>28</sub>O<sub>46</sub>," *Journal of Alloys and Compounds*, vol. 741, pp. 377-391, 2018.
- [12] J. Rehman *et al.*, "Structural, magnetic and dielectric properties of terbium doped NiCoX strontium hexagonal nano-ferrites synthesized via micro-emulsion route," *Ceramics International*, vol. 42, no. 7, pp. 9079-9085, 2016.
- [13] T. Kaur, J. Sharma, S. Kumar, and A. K. Srivastava, "Optical and multiferroic properties of Gd-Co substituted barium hexaferrite," *Crystal Research and Technology*, vol. 52, no. 9, p. 1700098, 2017.
- [14] L. Shlyk, S. Strobel, B. Farmer, L. De Long, and R. Niewa, "Coexistence of ferromagnetism and spin glass freezing in the site-disordered kagome ferrite SrSn<sub>2</sub>Fe<sub>4</sub>O<sub>11</sub>," *AIP Advances*, vol. 8, no. 5, 2018.
- [15] S. Atiq, M. Faizan, A. H. Khan, A. Mahmood, S. M. Ramay, and S. Naseem, "Co-existence of magnetic and electric ferroic orders in La-substituted BiFeO<sub>3</sub>," *Results in Physics*, vol. 12, pp. 1269-1275, 2019.
- [16] A. Elahi, M. Ahmad, I. Ali, and M. Rana, "Preparation and properties of sol-gel synthesized Mg-substituted Ni<sub>2</sub>Y hexagonal ferrites," *Ceramics International*, vol. 39, no. 2, pp. 983-990, 2013.
- [17] M. H. Habibi and M. H. Rahmati, "Fabrication and characterization of ZnO@ CdS core-shell nanostructure using acetate precursors: XRD, FESEM, DRS, FTIR studies and effects of cadmium ion concentration on band gap," *Spectrochimica Acta Part A: Molecular and Biomolecular Spectroscopy*, vol. 133, pp. 13-18, 2014.
- [18] F. Song, X. Shen, J. Xiang, and Y. Zhu, "Characterization and magnetic properties of Ba<sub>x</sub>Sr<sub>1-x</sub>Fe<sub>12</sub>O<sub>19</sub> (x= 0–1) ferrite hollow fibers via gel-precursor transformation process," *Journal of alloys and compounds*, vol. 507, no. 1, pp. 297-301, 2010.
- [19] A. Majeed *et al.*, "Structural elucidation and magnetic behavior evaluation of rare earth (La, Nd, Gd, Tb, Dy) doped BaCoNi-X hexagonal nano-sized ferrites," *Journal of magnetism and magnetic materials*, vol. 408, pp. 147-151, 2016.
- [20] A. Ohlan, K. Singh, A. Chandra, and S. K. Dhawan, "Microwave absorption behavior of core-shell structured poly (3, 4-ethylenedioxy thiophene)- barium ferrite nanocomposites," *ACS applied materials & interfaces*, vol. 2, no. 3, pp. 927-933, 2010.
- [21] I. El-Mahallawi *et al.*, "Influence of nanodispersions on strength-ductility properties of semisolid cast A356 Al alloy," *Materials Science and Technology*, vol. 26, no. 10, pp. 1226-1231, 2010.
- [22] V. Turchenko *et al.*, "Features of crystal structure and dual ferroic properties of BaFe<sub>12-x</sub>Me<sub>x</sub>O<sub>19</sub> (Me= In<sup>3+</sup> and Ga<sup>3+</sup>; x= 0.1–1.2)," *Journal of Magnetism and Magnetic Materials*, vol. 464, pp. 139-147, 2018.
- [23] L. J. Berchmans, R. K. Selvan, P. S. Kumar, and C. Augustin, "Structural and electrical properties of Ni<sub>1-x</sub>MgxFe<sub>2</sub>O<sub>4</sub> synthesized by citrate gel process," *Journal of Magnetism and Magnetic Materials*, vol. 279, no. 1, pp. 103-110, 2004.